# STRONGLY NON-LINEAR ENERGETIC PARTICLE DYNAMICS IN ASDEX UPGRADE SCENARIOS WITH CORE IMPURITY ACCUMULATION

PH. LAUBER[1], B. GEIGER[1], G. PAPP[1], G. POR[2], L.GUIMARAIS[3], P. ZS. POLOSKEI[1], V. IGOCHINE[1], M. MARASCHEK[1], G. I. POKOL[2], T. HAYWARD-SCHNEIDER[1], Z. LU[1], X. WANG[1], A. BOTTINO[1], F. PALERMO[1], I. NOVIKAU[1], A. BIANCALANI[1] G.CONWAY[1], THE ASDEX UPGRADE TEAM AND THE EUROFUSION ENABLING RESEARCH 'NAT' AND 'NLED' TEAMS[4]
[1]MPI für Plasmaphysik, Garching, Germany; email: philipp.lauber@ipp.mpg.de
[2]Institute of Nuclear Techniques, Budapest University of Technology, Budapest, Hungary
[3]Instituto de Plasmas e Fusao Nuclear, IST, Universidade de Lisboa, Lisboa, Portugal
[4] see references [1, 2]

Email of corresponding author: philipp.lauber@ipp.mpg.de

**Abstract**

In 2017 a new scenario on ASDEX Upgrade for the dedicated investigation of energetic particle (EP) physics has been developed. This scenario is unique in two aspects: firstly, the neutral beam (NB) induced fast-ion beta is comparable to the background plasma $\beta$, and secondly, the ratio of the fast ion energy to the thermal background is of the order 100. At ASDEX Upgrade we reach this previously unexplored regime by NB off-axis heating only and by letting impurities accumulate in the core. Due to strong radiation losses the background temperatures and pressures of both ions and electrons stay low, despite 2.5 − 5MW NB heating. In the stable flat top phase an unprecedented number of various EP-driven instabilities (despite $v_{\mathrm{EP}}/v_{\mathrm{Alfvén}} \approx 0.4 \ll 1$) is simultaneously observed: EP-driven geodesic acoustic modes (EGAMs), beta-induced Alfvén eigenmodes (BAEs), reversed shear Alfvén eigenmodes (RSAEs) and toroidal Alfvén eigenmodes (TAEs), that are modulated by transient $q = 2$ sawtooth-like crashes, NTMs and ELMs. The physics reasons for this strong mode activity are discussed. Bicoherence analysis using an advanced toolset for non-stationary processes reveals that non-linear coupling processes between different frequency bands exist. E.g. TAE bursts are observed to trigger the onset of EGAMs which indicates coupling of these modes via the velocity space (EP avalanches) and via mode-mode coupling processes. A gyrokinetic analysis is carried out to identify the various modes and to understand their existence in various phases of the experiment, especially for EGAMs that require global electromagnetic modeling including anisotropic EP distribution functions.

## 1. INTRODUCTION

Predicting the self-organised state of a burning fusion plasma is an ongoing challenge for fusion research. In order to validate theoretical and numerical models, the comparison with present day experiments is an important element despite the fact that not all the crucial parameters can be matched simultaneously. Therefore, theory-driven experiments outside well explored parameter regimes can serve as important cross-check for the capability of the models with respect to physics that is expected to play a role for a comprehensive understanding of burning plasma physics.

In the last years DIII-D experiments reported stiff energetic particle (EP) transport when carrying out an on-axis neutral beam (NB) heating power scan during the ramp-up phases. A broad spectrum of toroidal Alfvén eigenmodes (TAEs) and reversed shear Alfvén eigenmodes (RSAEs) is found to be responsible for a phase-space dependent onset of strong EP transport that leaves the EP and background profiles unchanged despite a further increase of the NB power [3, 4] confirming the theoretical picture of resonance broadening theory [5, 6]. Due to the tungsten wall in ASDEX Upgrade (AUG) the NB heating power during ramp-up is limited, although similar small-amplitude TAEs and RSAEs in the low power ($\leq$ 5MW) on-axis heating cases are found [7]. The NB induced excitation of AEs in the flat top phases is difficult since for high current usually the damping dominates over the sub-Alfvénic drive via the $v_{EP} = v_A/3$ resonance ($v_A$: Alfvén velocity). However, for low current cases both DIII-D and AUG report beam driven AE activity with moderate EP redistribution [4, 8].

In the case of off-axis heating, the two experiments differ: whereas DIII-D reports a physics picture similar to the on-axis heating cases, in AUG the observed mode spectrum is dominated by strongly chirping BAEs (beta induced AEs) [9, 10]. Until very recently for the so-called beta-induced Alfvén-Acoustic mode [11, 12], DIII-D reports chirping events to be very rare [13]. In the case of super-Alfvénic beams chirping events are more common, as reported for NSTX[14], MAST[15, 16] and JT-60U[17, 18].

In order to understand the differences in mode spectrum and the non-linear behaviour, in this paper we report experiments from ASDEX Upgrade that are dedicated to a previously unexplored corner of the parameter space:

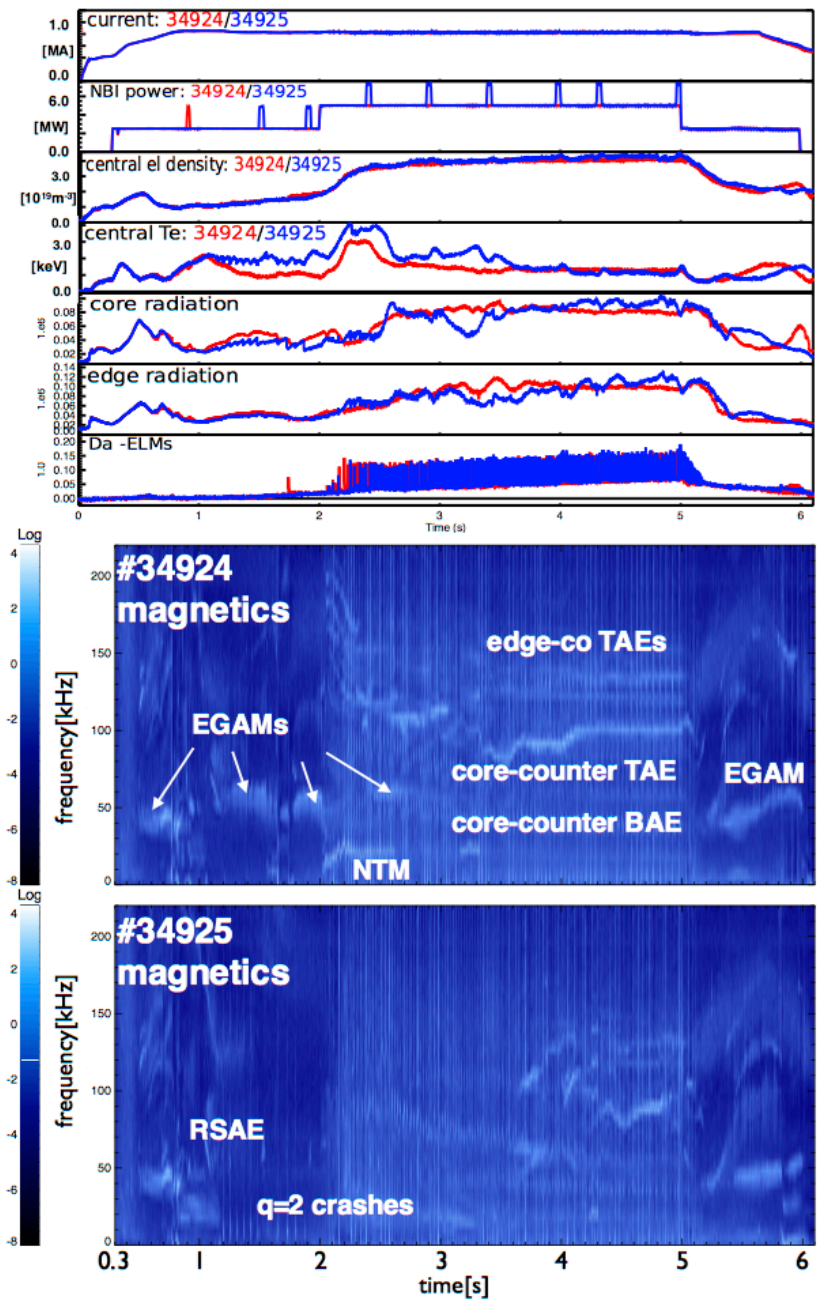


*FIG. 1. Time evolution of the main discharge parameters and comparison of the magnetic fluctuations of the pair of AUG discharges* #34924/#34925

large ratios ($\mathcal{O} \sim 1$) of the neutral-beam-generated energetic particle $\beta = 2\mu_0 p/B^2$ to the background plasma $\beta$ are established simultaneously with a large ratio of the EP energy to the thermal plasma temperature $93\ keV/1\ keV \approx \mathcal{O}(100)$.

At AUG we reach this regime by NB off-axis heating only and by letting impurities accumulate in the core. Due to the radiation losses the background temperatures and pressures of both ions and electrons stay low, despite 2.5 – 5 MW NB heating. In fact, in some phases of the discharge hollow electron temperature profiles develop. In order to avoid infernal modes (that typically develop when $q$ drops below 2 in the core and $q_{95}$ below 4) the current is limited to 800 kA with $B = -2.5$ T. This leads to a stable flat top phase with an unprecedented number of various EP-driven instabilities (despite $v_{EP}/v_{Alfvén} \approx 0.4 \ll 1$): EP-driven geodesic acoustic modes (EGAMs), BAEs, RSAEs and TAEs that are modulated by transient $q = 2$ sawtooth-like crashes, NTMs and ELMs.

The existence of this scenario in this peculiar parameter space opens the path to the exploration of various questions relevant for linear and non-linear theory and modeling. Firstly, the understanding of the linear onset conditions, in particular for the (electromagnetic) EGAMs serves as an important global test for gyrokinetic or MHD-hybrid codes. Secondly, the conditions for the large-amplitude mode bursting can be investigated and compared to theoretical models. Next, the modes' interaction via phase-space and mode-mode coupling shows unique signatures that help to verify, quantify and predict their respective importance in various plasma conditions. Finally, the question of background ion heating by EGAMs [20, 21] and the EGAMs' influence on the background turbulence [19] can be addressed. In this paper we will describe the basic physics picture of this scenario and include the status of the modeling that has been started so far.

## 2. EXPERIMENTAL RESULTS

The pair of discharges #34924 and #34925 is chosen to demonstrate the overall physics picture. In fig.1 the time evolution of important parameters is plotted together with the magnetic fluctuation spectrogram as given by the low-field side mid-plane magnetic pick-up coil *B31-14* measuring radial B-field perturbations. The first

beam (current drive source 7, 2.5MW, 93 $keV$) with the maximal off-axis injection angle $-7.13°$ with respect to the horizontal plane is switched on during ramp-up at $t = 0.3s$. The second beam (current drive source 6, 2.5MW, 93 $keV$) with a positive maximal inclination angle of 6.95° is added in the flat top current phase at $t = 2.0s$. On-axis diagnostic beam blips are applied to measure $T_i$, rotation and the FIDA (fast ion D-$\alpha$) emission. The magnetic fluctuation spectrum, in particular between 1.0s and 4.0s is very different in both discharges (see fig.1), despite similar current and density evolution. Clearly, the electron temperature and the core XUV radiation demonstrate the common finding in AUG that the lack of central heating leads to core impurity (mainly tungsten (W)) accumulation [22]. The difference between #34924 and #34925 can be attributed to the pre-conditioning of the machine: whereas the preceding discharge to #34924 had an ion-cyclotron heating (ICRH) phase with specific settings to maximise the amount of W impurities in the vessel, #34925 started from cleaner conditions, leading to conventional, non-hollow $T_e$ profiles in the flat top phase. This behaviour could be demonstrated in various discharges before (about 20 shots) and thus the scenario presented here is well reproducible except in operating phases directly after boronisation.

### 2.1. RAMP-UP PHASE

The current ramp-up phase of this scenario has been investigated best so far. In line with the discussion above, the first AUG discharge where EGAMs were observed has been tracked back to discharge #20492 in July 2005, in a time when the percentage of tungsten plasma facing components reached 75%. In 2014, the beam injection angle dependence of the EGAM has been investigated [23] and the non-linear EGAM radial mode structure evolution has been analysed for discharge #31213 using the soft X-ray emmission data [24]. Furthermore, a bicoherence study adopted to non-stationary processes has been performed focusing on the EGAM-TAE interaction found in #31213 [25]. Due to its unique features of non-linear EP-driven AE dynamics, #31213@0.84$s$ has been chosen as a 'base case' for linear and non-linear EP simulations within two European theory projects[26, 2, 1]. Both #34924 and #34925 exhibit a similar mode evolution pattern: large amplitude EGAMs exhibiting non-linear hook-up chirping are triggered by TAE bursts (see fig 2). The mode number analysis based on the magnetic magnetic pick-up coils shows that mode numbers $n = 0, m = 2$ for the mode at 50 kHz and $n = 1, m = 3$ for the mode at 125 kHz are found, supporting the identification of the fluctuations as EGAMs and TAEs. Various other diagnostics are used to determine the radial location and spatial structures: soft-x-ray emission cameras (SXR), reflectometry and interferometry. Unfortunately, the modes are not visible in the electron cyclotron emmission imaging diagnostics due to the low and inverted electron temperature profile. In addition, no fast ion losses could be measured so far, since the scenario has been in the development stage and thus a safe and optimised fast ion loss detector (FILD) position was not available. It should be noted however, that fast ion losses due to EGAMs have been observed in the ramp up phase of discharge #30383, that are probably caused by topological orbit changes (barely circulating to trapped) [27]. With optimised FILD settings this hypothesis will be further investigated in the future. Using the fast stepping frequency reflectometry data, the EGAM density perturbation has been found to peak at $s \approx 0.3$ with a radial extension at least from $s \approx 0.2-0.6$ where $s$ is defined as the square root of the normalised poloidal flux. This is supported by the SXR data. The magnetic perturbations are global and can be seen in nearly all magnetic pick-up coils. The measured peak amplitude $\delta n/n$ as determined by reflecometry is approximately $\lesssim 4\%$. A detailed analysis of the EGAM stability and existence will be carried out in section 3.2.

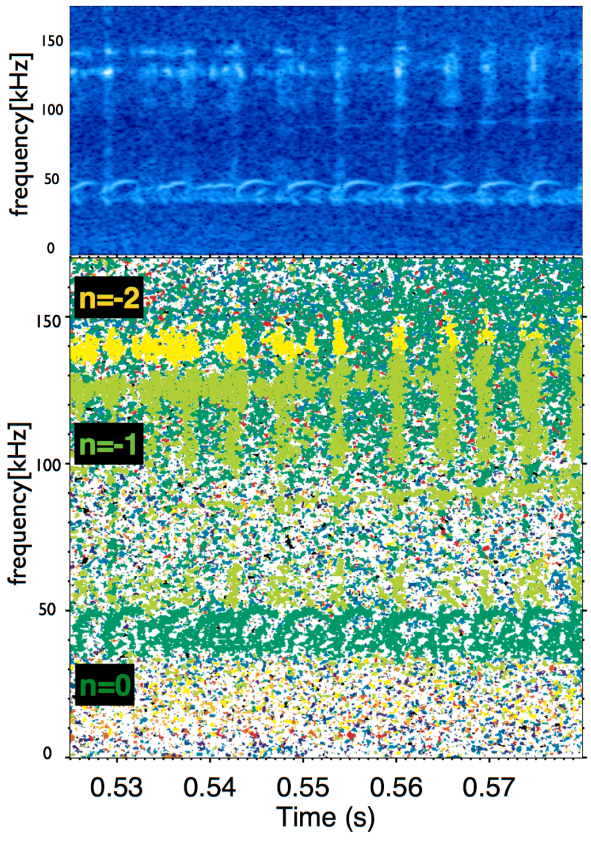


*FIG. 2. Time evolution the magnetic perturbation spectrum (B13-14 ) and the related mode number analysis of AUG discharge* #34924

The TAE mode has a similar radial localisation as the EGAM, i.e peaked in the plasma core, rotating in the electron diamagnetic direction. This means that a positive radial gradient of $F_{EP}$ must be present, similar to recent observations at NSTX [28]. The $q$-profile in this phase is reversed with $q_{min}$ approaching 2 at $t = 1.18s$ what can be inferred from a down-chirping $n = 1$ RSAE.

The existence of an EGAM requires an anisotropic distribution function near its resonance: it has been found that for NB injection geometry the strongest anisotropy occurs at 35 keV with $\Lambda = \mu B_0/E \approx 0.55$ or $\lambda = 0.7$ [24]. Given this information, the EGAM should be also excitable with lower beam energy and additional beams should influence its existence. Both points could be demonstrated experimentally. Reducing the beam voltage to 65keV and thus halving the beam power still allowed us to excite EGAMs (#32327) while the TAEs disappear, as expected from a resonance analysis. The modes' reaction to on-axis diagnostic beam blips reveals information about the drive mechanism: whereas in the presence of the off-axis beam, the on-axis beam blip (60keV) shifts the onset EGAM frequency according to a higher background temperature, the TAE bursts are completely suppressed (see fig 3). When analysing the NBI distribution function using the TRANSP/NUBEAM package [29] one can see that at the modes' peak position ($s = 0.3$) the intersection of the resonance lines with the gradients of the distribution function in velocity space remains practically unchanged (see fig.3, bottom right). Instead, the radial gradient is substantially flattened in the core region (see fig.3, bottom left), indicating that the TAEs tap a substantial amount of energy from the radial gradients. On the contrary, the EGAMs become even stronger during the beam blip, showing that the EP density itself (30% higher) is influencing its saturation amplitude. Within this argumentation the triggering of the EGAM by the TAE can also be understood: the TAE bursts flatten the off-axis peaked density and thus move EP density towards the plasma core, triggering the EGAM chirp. In addition to the triggering mechanism, a non-linear (quadratic) interaction between the two frequency bands can be detected with high confidence by performing a filtered bicoherence analysis for non-stationary processes [25]. Since the mode numbers are $n = 0, -1$ and $\omega_{TAE} \approx 2\omega_{EGAM}$ (#31216) or $\omega_{TAE} \approx 3\omega_{EGAM}$ in discharge #32388 [25], non-linear mode-mode coupling processes are involved in the non-linear evolution of the modes.

## 2.2. FLAT TOP

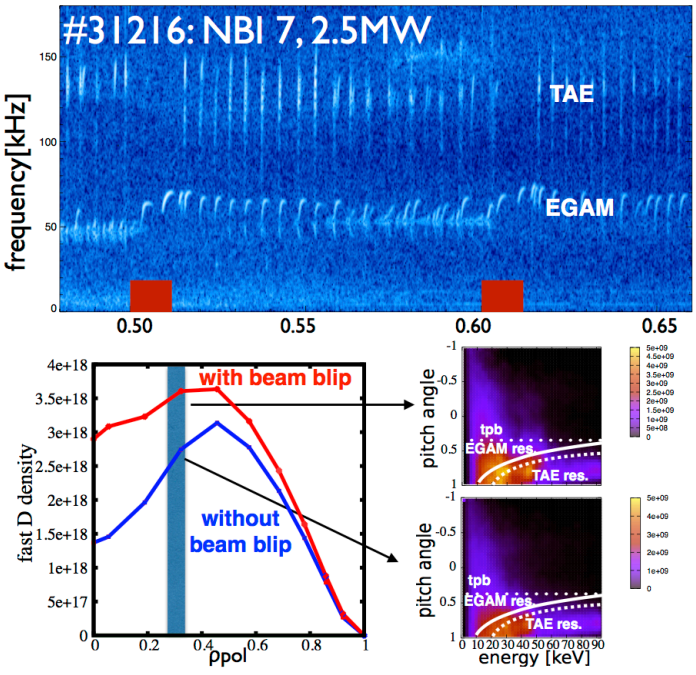


*FIG. 3. Top:time evolution the magnetic perturbation spectrum (B13-14) #31216. The red boxes represent the timing of on-axis 60keV beam blips. On the bottom left, the radial density profiles of the NBI ions as calculated by TRANSP/NUBEAM are shown for two discharges with (#31216, red) and without (#31215, blue) beam blips at $t = 0.51s$. On the right, the phase space densities of the NBI ions for the two cases at $s = 0.3$ (unit: $m^{-3}keV^{-1}$); the dotted line marks the trapped passing boundary (tpb), the dashed and solid lines the main resonance conditions for TAEs and EGAMs.*

After the $q = 2$ surface enters the plasma, the two discharges start to develop differently: whereas #34924 shows a stable EGAM phase with hollow $T_e$ profiles interrupted by two strong reconnection events at $1.65s$ and $1.75s$, #34925 develops regular, sawtooth like crashes at the $q = 2$ surface. Depending on the size of the crashes, i.e. the distance between the two $q = 2$ surfaces and their radial locations, the impurities are flushed out from the core restoring monotonic $T_e$ profiles or leading to large reconnection events that flatten the whole core region. Small crashes and simultaneous EGAM activity have been observed in cases with slightly higher flat top currents (1MA, #32388) supporting this physics picture. An interesting feature in this phase is the appearance of the 1st upper harmonic EGAM frequency in the spectrum. Bicoherence analysis confirms a strongly anharmonic (i.e. quadratic ) component in the EGAM oscillation. The stable EGAM phase in #34924 (just interrupted by one reconnection event) is an ideal phase to investigate the influence of EGAMs on the background turbulence. Unfortunately, the beam blips in the phase failed due to a technical issue, but further optimised modula-

tion experiments (ECRH,NBI) will help to provide data for analysing the transport properties in the presence of EGAMs, but also for understanding the influence of the beam anisotropy on the zonal flow generation [19, 30, 31].

### 2.3. FLAT TOP, ADDING SECOND BEAM SOURCE

Switching on the second $2.5MW$ beam at $2.0s$ moves the plasma to H-mode and triggers a transient NTM at the $q = 2.5@s = 0.65$ surface with the mode numbers $n = 2, m = 5$. The modulation effect of ELM bursts can be traced deep into the plasma core since it modulates not only the NTMs but also AEs propagating in the electron diamagnetic direction that require a positive radial gradient as drive. The second beam provides initially enough central heating to remove the impurities and the hollow $T_e$ profile after 200ms, that is exactly the TRANSP/NUBEAM calculated beam slowing down time. Also the previously peaked density profile becomes flat. Another $200ms$ later, the accumulation starts again and leads to a stable phase with hollow $T_e$ and linear $T_i$ where $T_i(0) \approx 2keV$ as measured by the beam blips in #34925. The reduced plasma beta is responsible for the NTM disappearing after $t > 2.6s$. During this phase not only edge localised TAEs (co-propagating) are unstable, but simultaneously also EGAMs, BAEs and core TAEs (counter-propagating). In addition, all core modes are bursting and they are synchronised by a similar phase space coupling mechanism as described above for the TAE-EGAM coupling (see fig 4). However, in this case no significant bicoherence can be detected, indicating that the modes' amplitudes are too small to show any quadratic mode-mode coupling signatures. It should be noted that the TAE just below 120kHz is not exactly at $2 \cdot f_{BAE}$, and that the onset between the BAE and TAE/EGAM is delayed by $\sim$ 0.5ms. This kind of cross coupling between different types of modes has not been reported by other experiments so far, in particular in the presence of sub-Alfvénic co-passing NBI drive. It is remarkable that no 'steady-state' non-linear mode behaviour is found in the onset phase, instead the modes immediately burst. This finding seems to be consistent with recent theoretical work on the chirping onset conditions [11]: the level of turbulence at the modes' position is assumed to be very small (small gradients of both $T_e$ and $T_i$; shear is reversed) whereas the collisionality is increased due to low $T_e$. According to ref. [11] these conditions can prevent steady state solutions and lead to chirping mode behaviour. A quantitative evaluation of various chipring scenarios at AUG is planned for the near future. In addition to the coupling between TAEs, BAEs and EGAMs, there is a non-linear interaction (as proven by bicoherence analysis) of these modes with the NTM, similar to ref. [32]. Later in the flat top phase ($3.6s < t < 4.0s$), a strong $n = -2$ counter- propagating TAE mode is present at $\approx$ 95kHz. It is visible in all SXR channels from the core to the edge, peaking at $s \approx 0.3$ and its growth rate as determined from the magnetic coil signal during one of its bursts is $\gamma/\omega \geq 20\%$. This mode shows non-linear interactions with other TAEs propagating in the ion diamagnetic directions (see fig.5), i.e. two $n = 4$ TAEs at $138kHz$ (and to a weaker extent at $120kHz$) that are localised closer to the plasma edge since they are modulated by ELMs. The frequencies match when taking into account that one has to subtract/add the toroidal plasma rotation frequency, which is about $7kHz$, as measured by beam blips in #34925. The $n = -2$ BAE mode at $f = 42\,kHz$, that is modulated by ELMs and therefore also

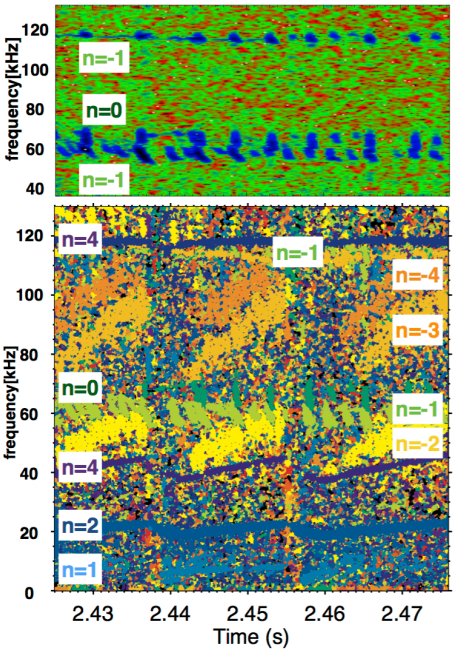


*FIG. 4. Spectrogram of a central SXR channel (J_051, tangential to $s \approx 0.3$) (top) and toroidal mode number spectrum (bottom) of #34924.*

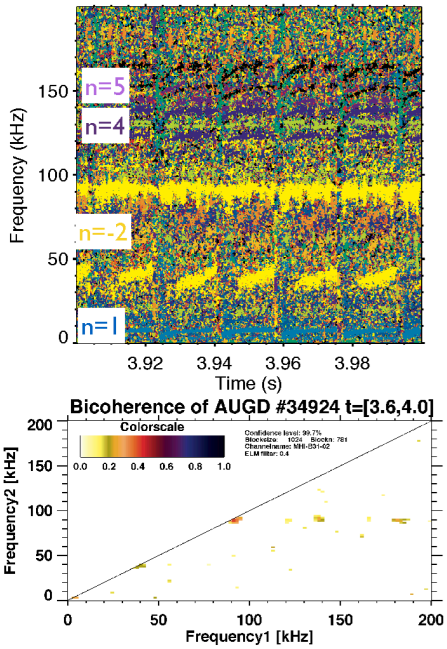


*FIG. 5. Mode number analysis (top) and bicoherence analysis (bottom) for discharge* #34924.

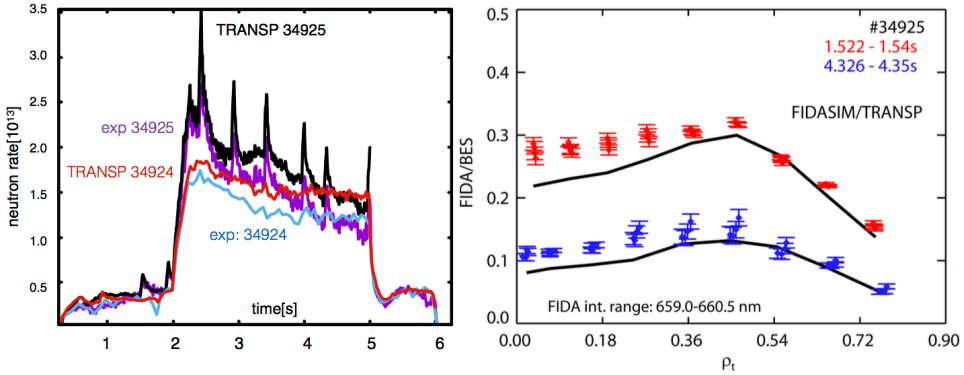


*FIG. 6. Left: TRANSP calculated and experimental neutron rates. The uncalibrated experimental signal has been matched to the TRANSP runs in phases with no visible mode activity. Right: the fast ion D-α signal shows moderate radial redistribution*

radially further outside than the core-peaking TAE, has no significant bicoherence with the strong $n = -2$ TAE, since there is no frequency match between the modes and their harmonics. In addition, the modes at 42 and 95 $kHz$ exhibit strong self-interaction that is visible on the diagonal of the bicoherence plot.
Fig.6 addresses the overall EP transport properties of the two discharges. Unfortunately, in #34924 the beam blips failed after $t > 0.9s$, and in #34925 the blip occurred in a phase with weak mode activity. Nevertheless, a weak flattening of the EP distribution function is observed. Note, that the peak mode activity in terms of $\delta B/B$ in #34924 is at least a factor of 6 larger than in #34925. The neutron rates show a deviation of $\lesssim 20-30\%$ TRANSP predictions. This relatively small deviation despite strong mode activity is due to the fact that the strongest modes are counter-propagating AEs that gain their energy from the inward-moving EPs.

## 3. MODELING

Here we start to describe some of the key physics elements that are needed to understand the differences between #34924/25 and other discharges that do not show strongly unstable modes. Various other ongoing modeling efforts are reported in separate publications.

### 3.1. ALFVÉN MODES

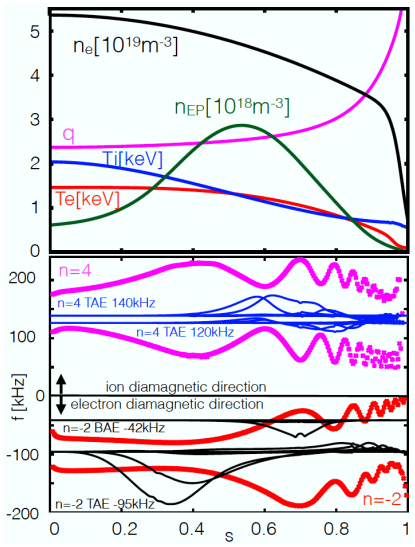


*FIG. 7. Profiles (top) and kinetic shear Alfvén spectra (bottom) inlcuding global unstable modes for discharge #34924 at 3.6s*

The physics reason for the appearance of this interesting fluctuation spectrum is the fact that ion Landau damping becomes exponentially small, whereas the slowing down time for the beam ions only decreases with $T_{thermal}^{-3/2}$. Also electron Landau damping decreases linearly with decreasing $\beta_e$. Due to the cold core and exclusive off-axis heating, both negative and a positive radial EP gradients develop, simultaneously destabilising modes that propagate in the ion and electron diamagnetic direction. In fig.7 the profiles for #34924@3.6$s$ (see fig.5 for the experimental mode spectrum) are given. The local and global analysis using the linear global gyrokinetic LIGKA code [33, 34] is also summarised in fig.7. The kinetic continuum for $n = -2$ and $n = 4$ are shown (positive/negative mode numbers indicate propagation in the ion/electron diamagnetic direction), together with the eigenmode structures (arbitrary units) at their respective frequencies. Four simultaneously unstable mode are found: a counter propagating global TAE at $f = 95\ kHz$ with a growth rate of 8%, a marginally unstable $n = -2$ BAE at 42 $kHz$ and two co-propagating $n = 4$ TAEs with $f = 140\ kHz$; $\gamma/\omega = 2.1\%$ and $f = 120\ kHz$; $\gamma/\omega = 1.4\%$. Whereas the frequencies and mode structures match the experiment, the growth rates for the counter-propagating modes are underestimated by LIGKA. Although the

EP anisotropy is taken into account, a sensitivity study will be necessary to understand this discrepancy.

### 3.2. EGAM

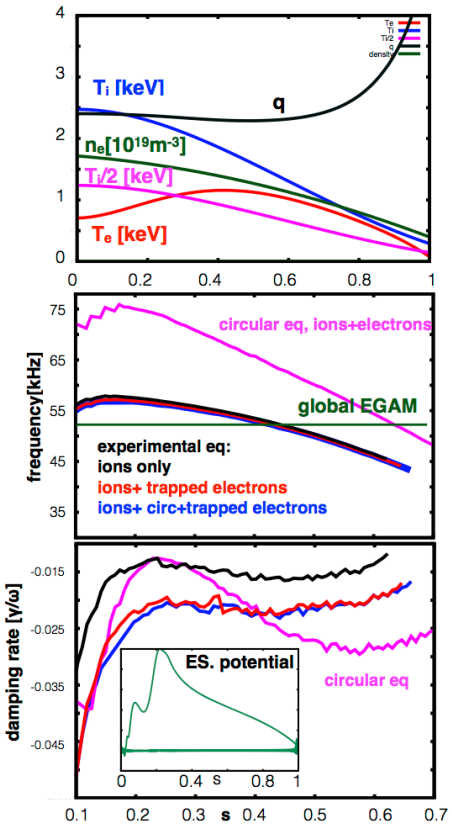


*FIG. 8. Typical profiles for phases with EGAM activity (top), local GAM frequency (middle) and local damping rate (bottom) in various approximations calculated with LIGKA. The global EGAM frequency and mode structure are included in the middle and lower plot.*

The modeling of EGAMs is a challenge since for a complete picture and comparison to the experiment a global, electromagnetic, gyro-kinetic model with realistic geometry and anisotropic $F_{EP}$ is necessary. Various aspects of EGAMs have been modeled previously, but so far never all aspects have been combined. We employ again LIGKA, that recently has been validated for kinetic GAM physics including finite Larmor radius and finite orbit width effects [35] . LIGKA can be used in various modes: it can be run locally and globally, with both analytically and numerically (based on HAGIS orbits and general $F_{EP}$) evaluated coefficients. In fig.8 the local GAM frequencies and damping rates $\gamma/\omega$ in the $k_\perp \varrho_i \rightarrow 0$ limit for the profiles given in fig.8, corresponding to typical experimental settings in #34924 or #31213 are given. As can be seen in fig.8, all the above mentioned elements play together to create a minimum in the radial damping profile around $s \approx 0.3$: going from a circular to a shaped equilibrium, taking into account 2nd order poloidal sidebands, and adding trapped electrons significantly changes the damping rates, as previously reported [36, 37, 38, 39, 40]. Various scans for $T_i$,$T_e$, $T_e/T_i$ and $q$ (not shown here) representing phases where EGAMs are absent or become marginally unstable show that mainly $q$ influences the overall damping, whereas $T_i$ and $T_e$ set the frequency, as expected from the analytical dispersion relation. However, unstable EGAMs are only found when the local GAM frequency matches the region of largest EP anisotropy (see fig.15 of ref [24]). This means that NBs with higher energy (e.g. in JT-60SA) should be able to drive EGAMs in the presence of higher background plasma temperature as long as the beam anisotropy matches the local GAM frequency, and $q \gtrsim 2$ (and possibly non-monotonic, as it is typical for advanced scenarios). The global EGAM mode (see fig.8) as driven by the $\partial F_{EP}/\partial \Lambda$ anisotropy is located close to the damping minimum i.e. $s = 0.3$. It has a frequency of 52 $kHz$, a growth rate of 10% and its radial mode width is comparable to the orbit width of the resonant co-passing ions. Its stable counterpart, the kinetic GAM has a similar mode structure but slightly higher frequency (55 $kHz$), as expected from the EGAM dispersion relation [41].

## 4. CONCLUSIONS AND OUTLOOK

After clarifying the basic and surprising properties of these discharges, various new efforts both experimentally and theoretically will follow: a better quantification of the fluctuations with optimised diagnostic settings and modulated heating will allow us to study the interaction of AEs, zonal modes and turbulence. This can serve as a validation opportunity for various non-linear analytical and numerical models. In addition, the observed onset of EP avalanches can be quantified. The findings can be extrapolated to future experiments, such as JET, JT-60SA or ITER. Finally, fusion-born $\alpha$ particles during a thermal quench may - due to low background temperatures - destabilise various AEs that could prevent the formation of problematic runaway currents.

**ACKNOWLEDGMENTS**

This work was partly performed within the framework of the EUROfusion Consortium and has received funding from the Euratom research and training programme 2014-2018 under grant agreement No 633053. Furthermore, funding from the EUROfusion Enabling Research work-package AWP15-ENR-09/ENEA-03 (NLED) and AWP15-ENR-09/IPP-01 (NAT) are acknowledged. The views and opinions expressed herein do not necessarily reflect those of the European Commission.

## REFERENCES


[1] Ph Lauber et al 2017 Wiki pages of the Eurofusion Enabling Research Project CfP-AWP17-ENR-MPG-01: Nonlinear interaction of Alfvénic and turbulent fluctuations in burning plasmas (NAT) URL `https://www2.ipp.mpg.de/ pwl/NAT/ENR_NAT.html`

[2] F Zonca et al 2015 Wiki pages of the Eurofusion Enabling Research Project CfP-AWP15-ENR-ENEA-03: Nonlinear Energetic Particle Dynamics (NLED) project URL `https://www2.euro-fusion.org/ERwiki/index.php?title=ER15-ENEA-03`

[3] Collins C S, Heidbrink W W, Austin M E, Kramer G J, Pace D C, Petty C C, Stagner L, Van Zeeland M A, White R B and Zhu Y B (DIII-D team) 2016 *Phys. Rev. Lett.* **116**(9) 095001

[4] Heidbrink W W, Collins C S, Podest M, Kramer G J, Pace D C, Petty C C, Stagner L, Van Zeeland M A, White R B and Zhu Y B 2017 *Physics of Plasmas* **24** 056109 (*Preprint* `https://doi.org/10.1063/1.4977535`)

[5] Dupree T H 1966 *The Physics of Fluids* **9** 1773–1782 (*Preprint* `https://aip.scitation.org/doi/pdf/10.1063/1.1761932`)

[6] Berk H, Breizman B, Fitzpatrick J and Wong H 1995 *Nuclear Fusion* **35** 1661

[7] Garcia-Munoz M, Classen I, Geiger B, Heidbrink W, Zeeland M V, kslompolo S, Bilato R, Bobkov V, Brambilla M, Conway G, da Graa S, Igochine V, Lauber P, Luhmann N, Maraschek M, Meo F, Park H, Schneller M, Tardini G and the ASDEX Upgrade Team 2011 *Nuclear Fusion* **51** 103013

[8] Geiger B 2018 *as presented at the 27th IAEA FEC, 22-27 October 2018, Gandhinagar (Ahmedabad) Gujarat, India.*

[9] Classen I G J, Lauber P, Curran D, Boom J E, Tobias B J, Domier C W, Jr N C L, Park H K, Garcia-Munoz M, Geiger B, Maraschek M, Zeeland M A V, da Graca S and the ASDEX Upgrade Team 2011 *Plasma Physics and Controlled Fusion* **53** 124018

[10] Lauber P, Classen I, Curran D, Igochine V, Geiger B, da Graa S, Garca-Muoz M, Maraschek M, McCarthy P and the ASDEX Upgrade Team 2012 *Nuclear Fusion* **52** 094007

[11] Duarte V N, Berk H L, Gorelenkov N N, Heidbrink W W, Kramer G J, Nazikian R, Pace D C, Podest M and Van Zeeland M A 2017 *Physics of Plasmas* **24** 122508 (*Preprint* `https://doi.org/10.1063/1.5007811`)

[12] Duarte V, Gorelenkov N, Schneller M, Fredrickson E, Podest M and Berk H 2018 *Nuclear Fusion* **58** 082013

[13] Heidbrink W 2014 *private communication*

[14] Fredrickson E 2006 *Phys. Plasmas* **13** 056109

[15] Sykes A, Akers R, Appel L, Arends E, Carolan P, Conway N, Counsell G, Cunningham G, Dnestrovskij A, Dnestrovskij Y, Field A, Fielding S, Gryaznevich M, Korsholm S, Laird E, Martin R, Nightingale M, Roach C, Tournianski M, Walsh M, Warrick C, Wilson H, You S, Team M and Team N 2001 *Nuclear Fusion* **41** 1423

[16] Pinches S D, Berk H L, Gryaznevich M P, Sharapov S E and Contributors J E 2004 *Plasma Physics and Controlled Fusion* **46** S47

[17] Kimura H, Kusama Y, Saigusa M, Kramer G, Tobita K, Nemoto M, Kondoh T, Nishitani T, Costa O D, Ozeki T, Oikawa T, Moriyama S, Morioka A, Fu G, Cheng C and Afanas'ev V 1998 *Nuclear Fusion* **38** 1303

[18] Shinohara K, Kusama Y, Takechi M, Morioka A, Ishikawa M, Oyama N, Tobita K, Ozeki T, Takeji S, Moriyama S, Fujita T, Oikawa T, Suzuki T, Nishitani T, Kondoh T, Lee S, Kuriyama M, Team J , Kramer G, Gorelenkov N, Nazikian R, Cheng C, Fu G and Fukuyama A 2001 *Nuclear Fusion* **41** 603

[19] Zarzoso D, Sarazin Y, Garbet X, Dumont R, Strugarek A, Abiteboul J, Cartier-Michaud T, Dif-Pradalier G, Ghendrih P, Grandgirard V, Latu G, Passeron C and Thomine O 2013 *Phys. Rev. Lett.* **110**(12) 125002

[20] Osakabe M 2014 *IAEA FEC EX/10-3*

[21] Sasaki M, Itoh K and Itoh S I 2011 *Plasma Physics and Controlled Fusion* **53** 085017

[22] Neu R, Dux R, Geier A, Kallenbach A, Pugno R, Rohde V, Bolshukhin D, Fuchs J C, Gehre O, Gruber O, Hobirk J, Kaufmann M, Krieger K, Laux M, Maggi C, Murmann H, Neuhauser J, Ryter F, Sips A C C, Stbler A, Stober J, Suttrop W, Zohm H and the ASDEX Upgrade Team 2002 *Plasma Physics and Controlled Fusion* **44** 811

[23] Lauber P 2015 *IAEA TM on Energetic Particles Vienna, Austria (2015)*

[24] Horvath L, Papp G, Lauber P, Por G, Gude A, Igochine V, Geiger B, Maraschek M, Guimarais L, Nikolaeva V, Pokol G and the ASDEX Upgrade Team 2016 *Nuclear Fusion* **56** 112003

[25] Poloskei P Z, Papp G, Pokol G I, Lauber P W, Wang X, Horvath L and the ASDEX Upgrade team 2017 *44th EPS Conference on Plasma Physics* **P5.179**

[26] Ph Lauber 2015 The NLED base case URL `https://www2.ipp.mpg.de/home/p/pwl/NLED_AUG/data.html`

[27] Nazikian R, Fu G Y, Austin M E, Berk H L, Budny R V, Gorelenkov N N, Heidbrink W W, Holcomb C T, Kramer G J, McKee G R, Makowski M A, Solomon W M, Shafer M, Strait E J and Zeeland M A V 2008 *Phys. Rev. Lett.* **101**(18) 185001

[28] Podesta M, Fredrickson E and Gorelenkova M 2018 *Nuclear Fusion* **58** 082023

[29] PPPL 2018 for TRANSP references see URL `https://w3.pppl.gov/tftr/transp/refs`

[30] Zarzoso D, del Castillo-Negrete D, Escande D, Sarazin Y, Garbet X, Grandgirard V, Passeron C, Latu G and Benkadda S 2018 *Nuclear Fusion* **58** 106030

[31] Lu Z X, Wang X, Lauber P, Fable E, Bottino A, Hornsby W, Zonca F and Angioni C 2018 *presented at the THEORY OF FUSION PLASMAS JOINT VARENNA - LAUSANNE INTERNATIONAL WORKSHOP, Villa Monastero, Varenna, Italy, August 27 - 31, 2018, to be submitted to PPCF 2018*

[32] Chen W, Qiu Z, Ding X T, Xie H S, Yu L M, Ji X Q, Li J X, Li Y G, Dong J Q, Shi Z B, Zhang Y P, Cao J Y, Song X M, Song S D, Xu M, Yang Q W, Liu Y, Yan L W and Duan X R 2014 *EPL (Europhysics Letters)* **107** 25001

[33] Lauber P, Günter S, Könies A and Pinches S D 2007 *Journal Of Computational Physics* **226** 447–465

[34] Lauber P 2013 *Physics Reports* **533** 33 – 68

[35] Lauber P and Lu Z X 2018 *presented at the THEORY OF FUSION PLASMAS JOINT VARENNA - LAUSANNE INTERNATIONAL WORKSHOP, Villa Monastero, Varenna, Italy, August 27 - 31, 2018, to be submitted to JPC 2018*

[36] Sugama H and Watanabe T H 2006 *Journal of Plasma Physics* **72**(06) 825–828

[37] Gao Z, Peng L, Wang P, Dong J and Sanuki H 2009 *Nuclear Fusion* **49** 045014

[38] Zonca, F and Chen, L 2008 *EPL* **83** 35001

[39] Zhang H S and Lin Z 2010 *Physics of Plasmas* **17** 072502 (*Preprint* `https://doi.org/10.1063/1.3447879`)

[40] Novikau I, Biancalani A, Bottino A, Conway G D, Gurcan D, Manz P, Morel P, Poli E and Di Siena A 2017 *Physics of Plasmas* **24** 122117 (*Preprint* `https://doi.org/10.1063/1.5003784`)

[41] Fu G Y 2008 *Phys. Rev. Lett.* **101**(18) 185002